SCIENCE CHINA
Earth Sciences

•RESEARCH PAPER•

February 2019 Vol.62 No.2: 451–458
https://doi.org/10.1007/s11430-018-9239-0

Field-observation for an anticyclonic mesoscale eddy consisted of twelve gliders and sixty-two expendable probes in the northern South China Sea during summer 2017

Yeqiang SHU[1], Ju CHEN[1], Shuo LI[2], Qiang WANG[1], Jiancheng YU[2†] & Dongxiao WANG[1*]

[1] *State Key Laboratory of Tropical Oceanography, South China Sea Institute of Oceanology, Chinese Academy of Sciences, Guangzhou 510301, China;*
[2] *State Key Laboratory of Robotics, Shenyang Institute of Automation, Chinese Academy of Sciences, Shenyang 110016, China*

Received January 11, 2018; revised May 13, 2018; accepted June 21, 2018; published online September 6, 2018

Abstract An intensive field observation experiment using 12 Chinese gliders equipped with conductivity-temperature-depth (CTD) sensors and 62 expendable CTD probes (XCTDs) was performed to investigate the 3-D structure and time evolution of an anticyclonic eddy in the northern South China Sea (NSCS). The observed results showed that the anticyclonic eddy had a horizontal radius of about 80 km at surface and a vertical depth of impact of more than 1000 m. The largest temperature and salinity anomalies compared with the averaged values of the temperature and salinity profiles were 3.5°C and 0.4 psu at 120 m depth, respectively. Combined analysis of altimeter sea level and water mass properties indicated that the anticyclonic eddy was shed from the Kuroshio loop current. The vertical axis of the anticyclonic eddy tilted from surface to the observed maximum depth (1000 m) along its translation direction against the 2000 m isobath. The center of the anticyclonic eddy remained in the region east of Dongsha Island for more than half a month. During this time, the long axis direction of the eddy changed from across the slope to along the slope. Then, the eddy moved southward along the 2000 m isobaths. Both the geostrophic current and temperature distribution revealed that the eddy intensity weakened during the observation period gradually. These observations indicated strong interaction between the anticyclonic eddy and the slope topography of Dongsha Island.

Keywords Anticyclonic mesoscale eddy, Glider, northern South China Sea

Citation: Shu Y, Chen J, Li S, Wang Q, Yu J, Wang D. 2019. Field-observation for an anticyclonic mesoscale eddy consisted of twelve gliders and sixty-two expendable probes in the northern South China Sea during summer 2017. Science China Earth Sciences, 62: 451–458, https://doi.org/10.1007/s11430-018-9239-0

1. Introduction

The underwater glider is a new type of autonomous vehicle that combines buoy and robot technologies (Niu et al., 2017). The glider moves horizontally using its wings and vertically by controlling its buoyancy, which requires only a small amount of energy; therefore it has a long cruise time and large observation area (Rudnick et al., 2004). A glider equipped with oceanic sensors can serve as a monitoring platform for ocean environment variables. With its high-resolution spatiotemporal sampling, the glider has been adopted widely in oceanographic research to understand the dynamics of oceanic processes, such as mesoscale eddies, submesoscale eddies, fronts, and western boundary currents (Leonard et al., 2010; Shu et al., 2016a; Ruan et al., 2017). Compared with the Slocum glider (Webb et al., 2001), Seaglider (Eriksen et al., 2001), and Spray glider (Sherman et al., 2001) designed by Americans in the early 21st century, the Sea-Wing glider (Yu et al., 2013) and the Petrel glider

* Corresponding author (email: dxwang@scsio.ac.cn)
† Corresponding author (email: yjc@sia.cn)

(Liu et al., 2017) developed by China are relatively recent arrivals in the study of oceanography.

The kinetic energy of mesoscale eddies (scales of tens to hundreds of km) is more than an order of magnitude greater than the mean kinetic energy over most of the ocean (Wyrtki et al., 1976; Richardson, 1983; Chelton et al., 2007). Studying the 3-D structure of the mesoscale eddies and their evolution are important for understanding mesoscale dynamics and the energy cascade among large-scale currents, mesoscale eddies, and submesoscale currents (Capet et al., 2008; Zu et al., 2013; Zhang et al., 2016). Influenced by local wind curl and the instability of the front induced by Kuroshio intrusion, the northern South China Sea (NSCS) is characterized as an area with high mesoscale eddy activities (Li et al., 1998; Chu and Fan, 2001; He et al., 2002; Wang et al., 2003; Wang D et al., 2008; Wang G et al., 2008; Nan et al., 2011; Xiu et al., 2010; Zu et al., 2013). Moreover, the mesoscale eddies in the SCS have a significant influence on the deep current (Zhang et al., 2013; Shu et al., 2016b). Previous studies have focused mostly on the general characteristics and the generation of submesoscale eddies in the NSCS (Chen et al., 2011; Zhuang et al., 2010; Li et al., 1998; Jia and Liu, 2004; Hu et al., 2012). Chu et al. (2014) investigated the 3-D structure of an anticyclonic eddy in the Xisha area based on the CTD observation. They didn't reveal the time evolution of 3-D structure of the anticyclonic eddy. Zhang et al. (2016) observed 3-D structure and time evolution of mesoscale eddies in the NSCS based on a "cross transect" mooring array. Their observations had a high resolution in both the vertical direction and time evolution. However, the horizontal resolution was not enough to show the fine structure of the mesoscale eddy in the horizontal plane.

The underwater glider offers full-scale sampling observation of mesoscale to submesoscale processes with a large spatial coverage and a high temporal resolution and can be used to observe the fine 3-D structure and its time evolution of mesoscale eddies. This study investigated the detailed structure and deformation of a temporarily stationary anticyclonic eddy in the NSCS using 12 Chinese Sea-Wing gliders and 62 expendable probes.

2. Glider network observations

2.1 Sea-Wing underwater glider

The Sea-Wing underwater glider was developed by the Shenyang Institute of Automation, Chinese Academy of Sciences, and is designed for observation of deep-sea environmental variables (Yu et al., 2011). The Sea-Wing glider has a compact attitude-regulating unit because of its individual pitch and roll attitude-regulating mechanism (Yu et al., 2011). The steady gliding motion parameters of the Sea-Wing glider are optimized to save energy and increase gliding range (Yu et al., 2013). The Sea-Wing underwater glider was sea tested from October 15, 2014, when it glided 1000 km during a duration of one month. After this test, the Sea-Wing underwater glider began to be applied to oceanographic studies (Qiu et al., 2015; Shu et al., 2016a).

2.2 Twelve gliders' network in the NSCS

A glider network observation experiment was carried out in the NSCS from July 14, 2017, to August 14, 2017. One of the research initiatives was to reveal the 3-D structure of an anticyclonic mesoscale eddy in the NSCS and improve understanding of mesoscale eddy dynamics. In the experiment, 12 Sea-Wing underwater gliders were deployed from the scientific research vessel Kexue (Figure 1b). The maximum observation depths of nine of the gliders were 1000 m, and that of the other three gliders was 300 m. All of the gliders were equipped with a Slocum Glider Payload conductivity-temperature-depth (CTD) sensor produced by Sea-Bird Electronics (SBE) in United States. The observation accuracies of the CTD are ±0.0003 S m^{-1} for electric conductivity, ±0.002°C for temperature, and ±0.1% for pressure, respectively. The sampling frequency was set to be 6 s^{-1} and

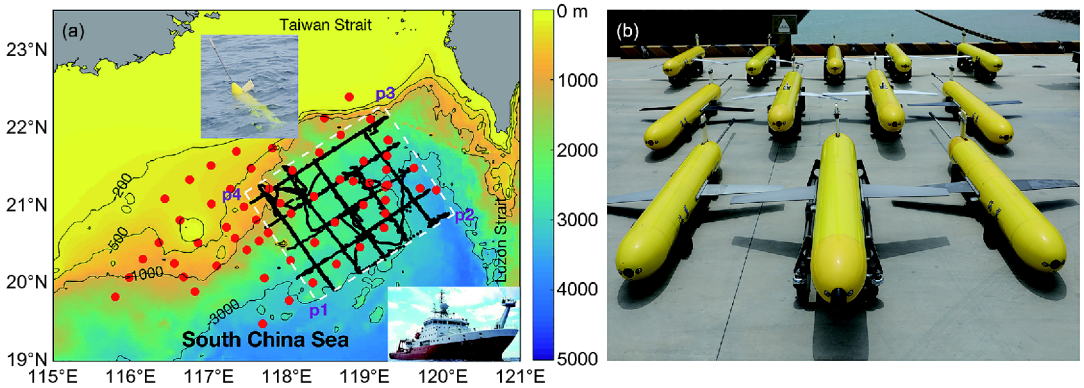

Figure 1 (a) The topography of the South China Sea. The red dots represent the 62 XCTD stations and the black dots are the glider trajectories. Bottom-right corner shows the vessel Kexue. (b) The 12 gliders used in the network observation experiment.

the vertical resolution was about 0.6 m. The glider observation region, in which each glider cruised repeatedly along a path, is shown in Figure 1a. During the experiment, we obtained 3720 profiles with an average horizontal resolution of 2.1 km along the glider trajectories and an average sampling frequency of each glider of 2.4 h.

2.3 Hydrographic survey

To obtain background hydrographic characteristics, 62 expendable CTD (XCTD) probes produced by Tsurumi Seiki Co. Ltd. in Japan were deployed in a larger domain than that of the gliders (Figure 1a). The type of the probes used in the observation experiment were XCTD-1 with the measuring depth of 1000 m and measuring time of 300 s under the ship speed within 12 knots. The observation accuracies of the XCTD are ±0.003 S m^{-1} for electric conductivity, ±0.02°C for temperature, and ±2% for depth, respectively. The vertical resolution of the XCTD observation was 1 m. The XCTD observations were executed between July 13 and July 22, 2017. The terminal observation depth of the XCTD probes was 1000 m. Basic quality control was performed for all *in situ* data used in this study as follows. Firstly, the obviously abnormities were removed. Secondly, we removed the temperature and salinity observations, where they were out of 2 (1.5) times of stand deviation when the temperature is larger (lower) than 15°C (Zeng et al., 2016a, 2016b). At last, both the temperature and salinity values were deleted when the vertical temperature gradient was larger than 0.3°C m^{-1}.

3. Anticyclonic eddy characteristics revealed by field observation experiment

3.1 Satellite observation of the anticyclonic eddy

The daily absolute dynamic topography (ADT) and surface geostrophic velocity from June to August 2017 were obtained from the AVISO gridded dataset to illustrate the time evolution of the anticyclonic eddy; the data were averaged using the nearest seven days (Figure 2). A Loop current appeared in the Luzon Strait on June 15 with the 1.15 m contour line of the ADT blending westward (Figure 2a). Afterward, the meander enhanced (Figure 2b) and an anticyclonic eddy was formed on July 29 (Figure 2c). Then the anticyclonic eddy shed from the Kuroshio and propagated westward with a translation speed of about 5.8 cm s^{-1} (Figure 2c–e). The anticyclonic eddy generally remained east of Dongsha Island for more than 15 days after it encountered the slope topography on July 13, 2017 (Figure 2e–g). During the period of July 13–27, 2017, the shape of the anticyclonic eddy changed where the elliptical long axis direction turned from approximately across the slope to along the slope (Figure 2e–g). The deformation of the anticyclonic eddy indicated that it might have interacted with the slope topography. After July 28, 2017, the anticyclonic eddy moved southwestward approximately against the 2000 m isobaths with a translation velocity of 4.2 cm s^{-1} (Figure 2g–i). The average radius of the anticyclonic eddy at the surface was about 80 km.

3.2 Anticyclonic eddy characteristics observed by XCTD

The temperature and salinity observed by the XCTD and the Glider CTD were validated each other before they were used to present the anticyclonic characteristics. The temperature and salinity (T-S) diagram of XCTD was in accordance with that of Glider CTD (Figure 3a and 3b). Moreover, there were twelve XCTDs overlapped the glider profiles in space within a 3-day window. The T-S diagram revealed by the twelve overlapped profiles of XCTDs and those of Glider CTDs show the similar properties of water mass (Figure 3c). Considering that the sensors of XCTD and Glider CTD were from different manufacturers, we believe that both of them are generally reliable. It should be noted that the XCTD probes were not equipped with a pressure sensor and the depth data were computed automatically from the elapsed time and empirical parameters, some uncertainties existed in the depth data derived by XCTD. However, the averaged temperature and salinity errors at the same depth of XCTDs relative to glider were small (not shown here).

The anomalies of temperature and salinity observed by XCTD were shown in Figure 4a and 4b. The anomalies were calculated by subtracting the climatologic values of the temperature and salinity in July derived from World Ocean Atlas 2013 (WOA13, https://www.nodc.noaa.gov/OC5/woa13/). Figure 4 shows that that there was an anticyclonic eddy northwest of the Luzon Strait. The maximum temperature anomaly, with values of more than 3.5°C, appeared in the thermocline, at ~120 m. Comparison with the climatologic salinity, the maximum salinity anomaly of the anticyclonic eddy, with a maximum value of about 0.4 psu, also appeared in the thermocline (Figure 4b). Salinity anomalies of the anticyclonic eddy were observed mainly above 200 m, with negative salinity anomaly in the mixed layer and large positive anomaly between beneath the mixed layer and 200 m depth.

The T-S scatter diagram of XCTD in the anticyclonic eddy area shown in Figure 5 is used to investigate the source of the water. The characteristics of the SCS water mass and the Kuroshio water mass were also represented as a reference by the respective T-S diagrams derived from historic Argo profiles in the Boxes shown in Figure 5. The properties of the Kuroshio water are obviously different from those of the SCS water. The Kuroshio water is warmer and more saline in

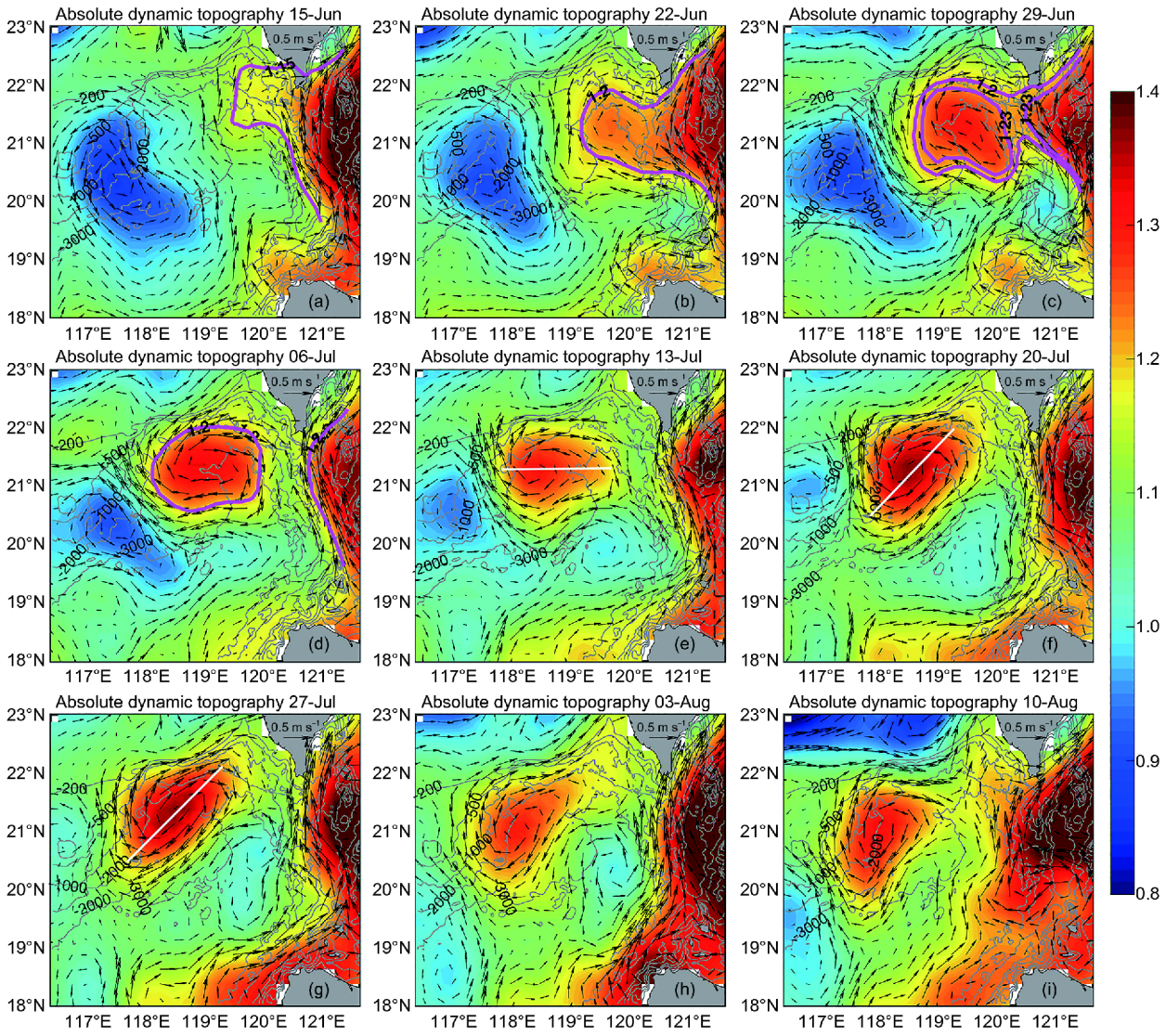

Figure 2 Time evolutions of the absolute dynamic topography (SLA; m) and geostrophic current (m s^{-1}) from June 15 to August 10, 2017. The gray lines are the 500, 1000, 2000, and 3000 m isobaths. The magenta lines show the 1.15 m isoline of the ADT in (a) and 1.2 isoline in (b)–(d). The white lines in (e)–(g) indicate the long-axis of the eddy.

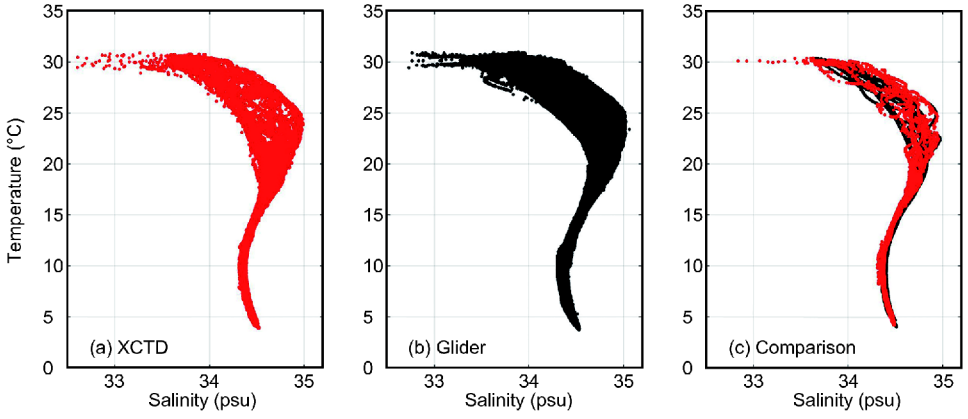

Figure 3 The diagrams of temperature and salinity. (a) XCTD, (b) Glider and (c) the comparison of XCTD (red dots) and Glider (black dots).

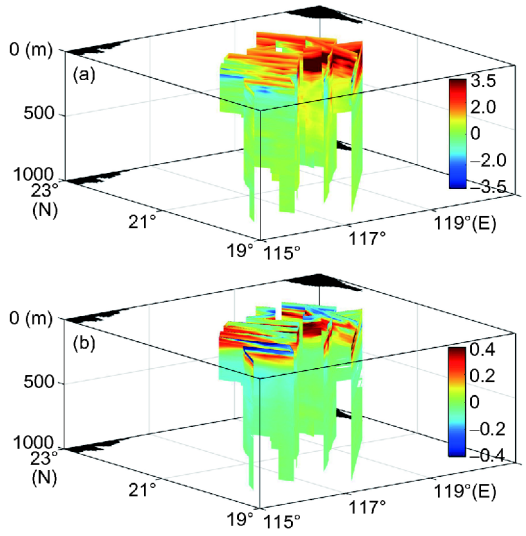

Figure 4 The XCTD observed temperature ((a); °C) and salinity ((b); psu) anomalies relative to the WOA13.

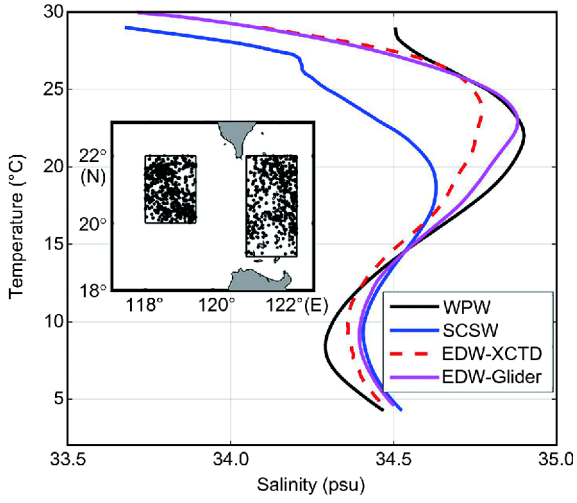

Figure 5 Mean T-S diagrams of water mass within and outside of the eddy. Blue and black lines show the results of the NSCS water and the Kuroshio water, respectively, computed based on historical Argo T-S profiles within the black boxes of the inset figure. Red-dashed line and magenta line show the results within the anticyclonic eddy derived from the XCTD probes and Gliders, respectively.

the upper layer, and colder and fresher in the intermediate layer than the SCS water. Both XCTD and Glider observed eddy water mass above 15°C of temperature had similar properties to the Kuroshio water and was significantly different from the SCS water. This further suggested that the source water of the eddy was from the Kuroshio (Shu et al., 2016a), and verified the eddy shed from Kuroshio as shown in Figure 2. Typically, an anticyclonic eddy generated by Kuroshio shedding is characterized by a positive salinity anomaly in the upper layer because of the higher salinity of Kuroshio water than of SCS water (Jia and Liu, 2004; Wang D et al., 2008; Shu et al., 2016a). The surface salinity of the anticyclonic eddy was lower than the climatologic SCS water, indicating that the anticyclonic eddy might entrained some surface SCS water (Zhang et al., 2017). It should be noted that there were some obvious differences of characteristic of water mass within the anticyclonic eddy observed by between the XCTD and Glider (Figure 5). Especially, below 15°C, the water mass observed by XCTD obviously differed from the SCS water, whereas the water mass observed by Glider was same to SCS water. Previous observation study had shown that the Kuroshio Current near the Luzon Strait is only confined to the upper 500 m layer (Lien et al., 2015). Moreover, Zhang et al. (2017) suggested that the anticyclonic eddy shed from the Kuroshio loop current only contained the Kuroshio water signals in the upper 300 m layer, which is coincident with the Glider observation (Figure 5). Therefore, the characteristics of water mass revealed by Glider should be more reliable than that by XCTD. The systematic error of XCTD can also be seen in Figure 3c, which might be due to the lag of the XCTD salinity probe in its rapid fall.

3.3 Interpretation of the 3-D structure and time evolution of the anticyclonic eddy revealed by the gliders

The temperature and salinity anomalies observed by the gliders are shown in Figure 6. The anomalies were derived by subtracting the climatologic temperature and salinity profiles and then using a Kriging interpolation method. According to the coverage of the glider observation, we separated the observation period into the three stages of July 14 to July 23, July 24 to August 3, and August 4 to August 14. The temperature anomaly indicates that the depth of impact of the anticyclonic eddy was more than the maximum observation depth, 1000 m (Figure 6a–c). The salinity anomaly appeared mainly from the surface to the depth of 200 m (Figure 6d–f). The largest temperature and salinity anomalies were approximately positive 3.5°C and 0.25 psu, respectively, and these were at a depth of about 120 m (not shown here), which was located in the typical thermocline in this area. Few temperature anomalies (~1.5°C) appeared in the surface throughout the entire observation period (Figure 6a–c). There was a negative salinity anomaly in the most area at the surface between July 14 and July 23, which also was observed by XCTD in the same period.

The distributions of the temperature and salinity anomalies shown Figure 6 also indicate the evolution of the anticyclonic eddy. During the observation period, the shape and position of the anticyclonic eddy changed significantly (Figure 6). To illustrate the time evolution of the anticyclonic eddy are shown in Figure 7a–c. In the first two stages, the center of eddy remained almost stationary, but the shape of the eddy changed. During stage 1, the direction of the long axis of the eddy in the horizontal plane was southeast-northwest, but during stage 2, the long axis direction turned

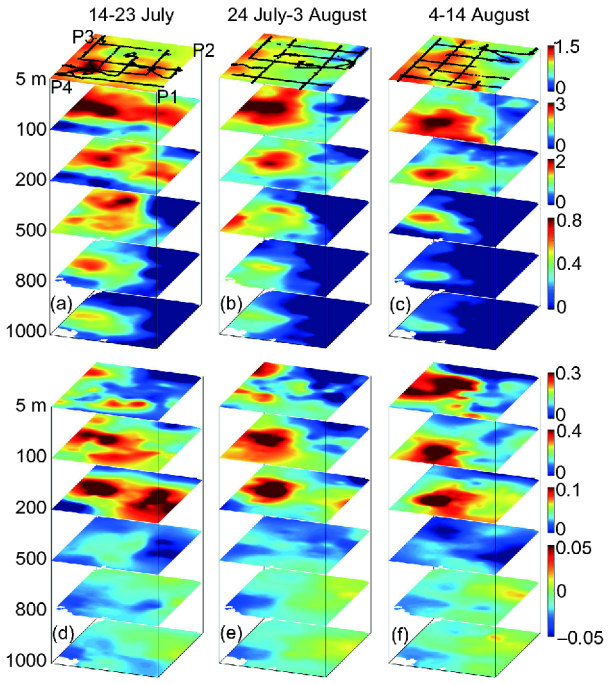

Figure 6 Glider-observed temperature ((a)–(c); °C) and salinity ((d)–(f); psu) anomalies at 0, 100, 200, 500, 800, and 1000 m (from top to bottom in each panel) in the three stages of July 14 to July 23, July 24 to August 3, and August 4 to August 14, 2017. P1, P2, P3, and P4 represent the positions shown in Figure 1a. Different ranges of the colorbars were used in the figure.

to become southwest-northeast (Figure 7a and b). Similar to the ADT result observed by AVISO, the change of the eddy shape observed by Glider further confirmed the interaction between the anticyclonic eddy and the slope topography. Yang et al. (2016) found that the propagation speed of eddies decreases in the Dongsha area because of the large topographic gradient. The slope topography in the Dongsha area hindered the westward propagation of the anticyclonic eddy and compressed the eddy in the cross slope direction. As a result, the anticyclonic eddy was trapped at this location for more than half a month and its long axis aligned with the 2000 m isobaths along the slope. In stage 3, the anticyclonic eddy moved southward along the 2000 m isobaths.

The anticyclonic eddy intensity weakened from stage 1 to stage 3, which can be found from the coverage range of positive temperature anomaly and of negative salinity anomaly at 1000 m depth (Figure 6). The decreased eddy intensity can also be seen from the evolution of the temperature distribution at 100 and 800 m depths shown in Figure 7. The geostrophic current was calculated from the thermal wind relation:

$$\frac{\partial u}{\partial z}=\frac{1}{\rho_0 f}\frac{\partial \rho}{\partial y}, \tag{1}$$

$$\frac{\partial v}{\partial z}=\frac{-1}{\rho_0 f}\frac{\partial \rho}{\partial x}, \tag{2}$$

where u and v represent zonal and meridional velocity, respectively, ρ_0 is reference density (1025 kg m^{-3}), ρ is potential density of sea water, and f is local Coriolis parameter. The reference depth was set to be at 1000 m where the velocity was assumed to be zero, which might underestimate

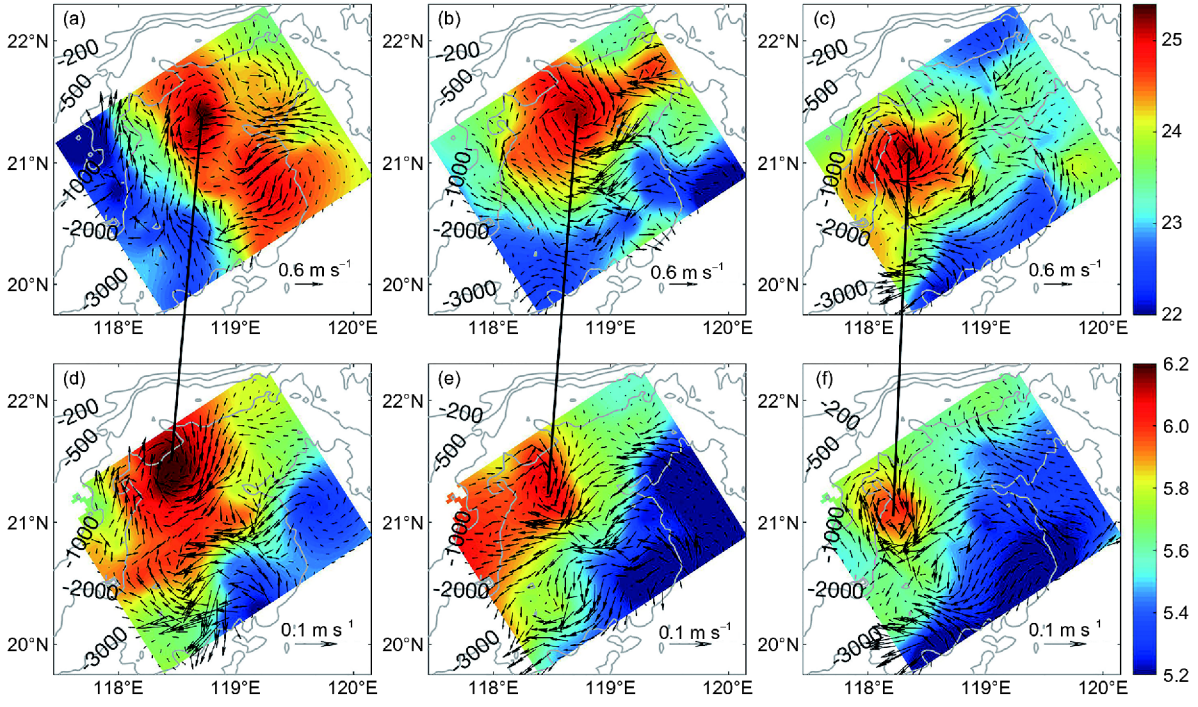

Figure 7 Glider-observed temperature (°C) at 100 m ((a)–(c)) and 800 m ((d)–(f)) in the three stages of July 14 to July 23 ((a), (d)), July 24 to August 3 ((b), (e)), and August 4 to August 14 ((c), (f)), 2017, respectively. Arrows denote the geostrophic current calculated from the Glider observed temperature and salinity. The black lines connected the eddy centers between 100 and 800 m depths.

the eddy intensity because the influence depth of the anticyclonic eddy was obviously larger than 1000 m (Figure 6). The geostrophic current at 100 m and 800 m depths show that the radium of the anticyclonic eddy reduced from stage 1 to stage 3 (Figure 7), also indicating that the intensity of the eddy decreased. The surface negative salinity anomaly disappeared during the stage 2 and stage 3 (Figure 6e–f). The reason might be because the horizontal convergence decreased when the intensity of anticyclonic eddy weakened, and the eddy tended to recover its original surface salinity in term of secondary circulation. Another characteristic of the anticyclonic eddy was that the vertical axis of the anticyclonic eddy titled, which can be seen from the position difference of the anticyclonic eddy centers between at 100 m and 800 depths (Figure 7). The titled direction from surface to deep layers was generally in coincidence with the propagation direction of the anticyclonic eddy. The tilted characteristic of the anticyclonic eddy in the NSCS was thought the cause of topographic β effect (Zhang et al., 2017).

4. Discussion and conclusion

We performed an intensive field observation experiment for an anticyclonic eddy in the NSCS using 12 gliders and 62 XCTDs. Using the glider and XCTD observation profiles, together with AVISO data, we presented the 3-D structure and time evolution of the anticyclonic eddy. The anticyclonic eddy had a horizontal radius of about 80 km and a vertical depth of impact of more than 1000 m. The largest temperature and salinity anomalies with values of 3.5°C and 0.4 psu, respectively, occurred at the depth of about 120 m. Analysis of the properties of water mass indicated that the eddy was originated from the Kuroshio shedding. The vertical axis of the anticyclonic eddy tilted from surface to deep layers along its translation direction, which was thought the cause of topographic β effect. During the observation period, the anticyclonic eddy was trapped in the area east of Dongsha Island for more than half a month. Interaction between the anticyclonic eddy and the slope topography occurred during this period. The direction of the long axis of the eddy changed approximately from across the slope to parallel to the slope. Subsequently, the eddy moved southward along the 2000 m isobaths. Both the geostrophic current and temperature distribution revealed that the eddy intensity weakened from stage 1 to stage 3.

This paper revealed interaction between the anticyclonic eddy and slope topography. However, how the anticyclonic eddy interacted with the topography was not investigated. Submesoscale processes are important for the energy dissipation of a mesoscale current (McWilliams, 2016). Ruan et al. (2017) found that the interaction between strong boundary currents and slope topography generates strong submesoscale turbulence beneath the thermocline. The gliders provided us with high-resolution observations, which enable study of submesoscale processes. Therefore, the energy translation between the large-scale current and the anticyclonic eddy, and the energy cascade and dispersion between the mesoscale eddy and submesoscale eddies should be investigated further.

Acknowledgements *This study benefited from the ADT data generated by DUACS and distributed by AVISO (ftp://ftp.aviso.oceanobs.com). This work was supported by the Strategic Priority Research Programs of the Chinese Academy of Sciences (Grant Nos. XDA11010302, XDA11040101), the National Natural Science Foundation of China (Grant Nos. 41521005, 41776036, 41476012, 61233013, 41576012 and 41776026), the Science and Technology Program of Guangdong, China (Grant No. 2016A020224003), and the National Key Scientific Instrument and Equipment Development Project (Grant No. 2013YQ16079303).*

References

Capet X, McWilliams J C, Molemaker M J, Shchepetkin A F. 2008. Mesoscale to submesoscale transition in the California current system. Part I: Flow structure, eddy flux, and observational tests. J Phys Oceanogr, 38: 29–43

Chelton D B, Schlax M G, Samelson R M, de Szoeke R A. 2007. Global observations of large oceanic eddies. Geophys Res Lett, 34: L15606

Chen G, Hou Y, Chu X. 2011. Mesoscale eddies in the South China Sea: Mean properties, spatiotemporal variability, and impact on thermohaline structure. J Geophys Res, 116: C06018

Chu P C, Fan C. 2001. Low salinity, cool-core cyclonic eddy detected northwest of Luzon during the South China Sea Monsoon Experiment (SCSMEX) in July 1998. J Oceanogr, 57: 549–563

Chu X, Xue H, Qi Y, Chen G, Mao Q, Wang D, Chai F. 2014. An exceptional anticyclonic eddy in the South China Sea in 2010. J Geophys Res-Oceans, 119: 881–897

Eriksen C C, Osse T J, Light R D, Wen T, Lehman T W, Sabin P L, Ballard J W, Chiodi A M. 2001. Seaglider: A long-range autonomous underwater vehicle for oceanographic research. IEEE J Ocean Eng, 26: 424–436

He Z, Wang D, and Hu J. 2002. Features of eddy kinetic energy and variations of upper circulation in the South China Sea (in Chinese). Acta Oceanol Sin, 21: 305–314

Hu J, Zheng Q, Sun Z, Tai C K. 2012. Penetration of nonlinear Rossby eddies into South China Sea evidenced by cruise data. J Geophys Res, 117: C03010

Jia Y, Liu Q. 2004. Eddy shedding from the Kuroshio bend at Luzon Strait. J Oceanogr, 60: 1063–1069

Leonard N E, Paley D A, Davis R E, Fratantoni D M, Lekien F, Zhang F. 2010. Coordinated control of an underwater glider fleet in an adaptive ocean sampling field experiment in Monterey Bay. J Field Robotics, 27: 718–740

Li L, Nowlin Jr. W D, Jilan S. 1998. Anticyclonic rings from the Kuroshio in the South China Sea. Deep-Sea Res Part I-Oceanogr Res Pap, 45: 1469–1482

Lien R C, Ma B, Lee C, Sanford T, Mensah V, Centurioni L, Cornuelle B, Gopalakrishnan G, Gordon A, Chang M H, Jayne S, Yang Y J. 2015. The Kuroshio and Luzon Undercurrent east of Luzon Island. Oceanography, 28: 54–63

Liu F, Wang Y, Wu Z, Wang S. 2017. Motion analysis and trials of the deep sea hybrid underwater glider Petrel-II. China Ocean Eng, 31: 55–62

McWilliams J C. 2016. Submesoscale currents in the ocean. Proc R Soc A, 472: 20160117

Nan F, He Z, Zhou H, Wang D. 2011. Three long-lived anticyclonic eddies in the northern South China Sea. J Geophys Res, 116: C05002

Niu W, Wang S, Wang Y, Song Y, Zhu Y. 2017. Stability analysis of hybrid-driven underwater glider. China Ocean Eng, 31: 528–538
Qiu C, Mao H, Yu J, Xie Q, Wu J, Lian S, Liu Q. 2015. Sea surface cooling in the Northern South China Sea observed using Chinese sea-wing underwater glider measurements. Deep-Sea Res Part I-Oceanogr Res Pap, 105: 111–118
Richardson P L. 1983. Eddy kinetic energy in the North Atlantic from surface drifters. J Geophys Res, 88: 4355–4367
Ruan X, Thompson A F, Flexas M M, Sprintall J. 2017. Contribution of topographically generated submesoscale turbulence to Southern Ocean overturning. Nat Geosci, 10: 840–845
Rudnick D L, Davis R E, Eriksen C C, Fratantoni D M, Perry M J. 2004. Underwater gliders for ocean research. Mar Tech Soc J, 38: 73–84
Sherman J, Davis R E, Owens W B, Valdes J. 2001. The autonomous underwater glider "Spray". IEEE J Ocean Eng, 26: 437–446
Shu Y, Xiu P, Xue H, Yao J, Yu J. 2016a. Glider-observed anticyclonic eddy in northern South China Sea. Aquat Ecosyst Health Manage, 19: 233–241
Shu Y, Xue H, Wang D, Chai F, Xie Q, Cai S, Chen R, Chen J, Li J, He Y. 2016b. Persistent and energetic bottom-trapped topographic Rossby waves observed in the southern South China Sea. Sci Rep, 6: 24338
Wang D, Xu H, Lin J, Hu J. 2008. Anticyclonic eddies in the northeastern South China Sea during winter 2003/2004. J Oceanogr, 64: 925–935
Wang G, Su J, Chu P C. 2003. Mesoscale eddies in the South China Sea observed with altimeter data. Geophys Res Lett, 30: 2121
Wang G, Chen D, Su J. 2008. Winter eddy genesis in the eastern South China Sea due to orographic wind jets. J Phys Oceanogr, 38: 726–732
Webb D C, Simonetti P J, Jones C P. 2001. SLOCUM: An underwater glider propelled by environmental energy. IEEE J Ocean Eng, 26: 447–452
Wyrtki K, Magaard L, Hager J. 1976. Eddy energy in the oceans. J Geophys Res, 81: 2641–2646
Xiu P, Chai F, Shi L, Xue H, Chao Y. 2010. A census of eddy activities in the South China Sea during 1993–2007. J Geophys Res, 115: C03012
Yang Y, Xing T, Wang Y, Sui J, Lei J, Zhou W, Wang Q, Qu L, Sui D. 2016. The topography effect on the sudden deceleration of the mesoscale eddy propagation speed around the Dongsha Islands in northern South China Sea. Aquat Ecosyst Health Manage, 19: 242–249
Yu J C, Zhang A Q, Jin W M, Chen Q, Tian Y, Liu C J. 2011. Development and experiments of the Sea-Wing underwater glider. China Ocean Eng, 25: 721–736
Yu J, Zhang F, Zhang A, Jin W, Tian Y. 2013. Motion parameter optimization and sensor scheduling for the Sea-Wing underwater glider. IEEE J Ocean Eng, 38: 243–254
Zeng L, Wang D, Chen J, Wang W, Chen R. 2016a. SCSPOD14, a South China Sea physical oceanographic dataset derived from *in situ* measurements during 1919–2014. Sci Data, 3: 160029
Zeng L, Wang D, Xiu P, Shu Y, Wang Q, Chen J. 2016b. Decadal variation and trends in subsurface salinity from 1960 to 2012 in the northern South China Sea. Geophys Res Lett, 43: 12181–12189
Zhang Z, Zhao W, Tian J, Liang X. 2013. A mesoscale eddy pair southwest of Taiwan and its influence on deep circulation. J Geophys Res-Oceans, 118: 6479–6494
Zhang Z, Tian J, Qiu B, Zhao W, Chang P, Wu D, Wan X. 2016. Observed 3D structure, generation, and dissipation of oceanic mesoscale eddies in the South China Sea. Sci Rep, 6: 24349
Zhang Z, Zhao W, Qiu B, Tian J. 2017. Anticyclonic eddy sheddings from Kuroshio loop and the accompanying cyclonic eddy in the northeastern South China Sea. J Phys Oceanogr, 47: 1243–1259
Zhuang W, Du Y, Wang D, Xie Q, Xie S. 2010. Pathways of mesoscale variability in the South China Sea. Chin J Ocean Limnol, 28: 1055–1067
Zu T, Wang D, Yan C, Belkin I, Zhuang W, Chen J. 2013. Evolution of an anticyclonic eddy southwest of Taiwan. Ocean Dyn, 63: 519–531

(Responsible editor: Dake CHEN)